# Reach-through effect in deep depletion TESS CCDs



2017 JINST 12 C04025

(http://iopscience.iop.org/1748-0221/12/04/C04025)

Published by IOP Publishing for Sissa Medialab

Received: *February 15, 2017*
Accepted: *March 30, 2017*
Published: *April 28, 2017*

Precision Astronomy with Fully Depleted CCDs
1–2 December 2016
Brookhaven National Laboratory, U.S.A.

# Reach-through effect in deep depletion TESS CCDs

**J. Villasenor,[a] G. Prigozhin,[a,1] J.P. Doty,[b] C. Lage,[c] S. Yazdi,[a] G. Ricker[a] and R. Vanderspek[a]**

[a] *MIT Kavli Institute for Astrophysics and Space Research, 70 Vassar St., Cambridge, MA, U.S.A.*
[b] *Noqsi Aerospace, Pine, CO, U.S.A.*
[c] *University of California Davis, Davis, CA, U.S.A.*

*E-mail:* gyp@space.mit.edu

Abstract: TESS CCDs are backside illuminated deep depletion devices fabricated on high resistivity p-type silicon substrate and thinned down to a thickness of 100 microns. In order to fully deplete the substrate and increase the near-IR efficiency, we apply a bias voltage to the back side of the device. A bias of -20V is sufficient to fully deplete this device, but overdepletion is desirable to minimize lateral diffusion which can blur images and in turn affect the photometric precision by increasing an area (and, hence, readout and background noise) associated with a given object of interest. For this reason much larger negative bias voltages have been applied. We can achieve sharper images with larger negative substrate voltage, but we also discovered an unexpected dramatic increase of the full well capacity beyond a certain threshold voltage. A large full well above 200,000e- is accompanied by poor charge conservation once the device is in the bloomed well condition. Both phenomena can be explained by backside voltage reaching through the substrate volume in the channel stop region, eliminating the barrier for holes, and dragging the floating channel stops to a more negative potential.

Keywords: Photon detectors for UV, visible and IR photons (solid-state); Photon detectors for UV, visible and IR photons (solid-state) (PIN diodes, APDs, Si-PMTs, G-APDs, CCDs, EBCCDs, EMCCDs etc)

[1] Corresponding author.



doi:10.1088/1748-0221/12/04/C04025

## Contents



2017 JINST 12 C04025

## 1 Introduction

TESS (Transiting Exoplanet Survey Satellite) is a spacecraft that will discover thousands of exoplanets through the transit method [1]. This method relies on precise photometry to detect the temporary reduction of the star light emission as an exoplanet crosses in front of its host star. The light dip from the transit can be on the order of a few 100 ppm, thus careful consideration must be given to all noise sources which will mask this effect. The motion of the star centroid within the focal plane can induce sufficient signal amplitude variations due to both intrapixel and interpixel nonuniformities, which can be large enough to hide shallow transits, so minimizing the PSF in the detector helps in reducing the noise.

TESS will use the MIT-LL CCID80 as the primary detector in its four cameras [2]. The CCID80 is a back illuminated frame transfer device which has a 2k $\times$ 2k array of 15 micron pixels in its Imaging Array (IA) section, and a similarly sized Frame Store (FS) section. It is a Backside Illuminated device built on a high resistivity p-type substrate, thinned down to 100 microns. Four of these CCDs are abutted to form an imaging field covering 24 $\times$ 24 field of view in combination with its f1.5 lens.

In order to increase the detection of earth size exoplanets, it is desirable to observe in the near infrared band. For example, M-type stars, for which earth size planets can be found, are better observed in the I-band. The quantum efficiency (QE) of photon absorption for regular CCDs is poor at those wavelengths, unless the absorption thickness is substantially increased, hence the requirement for deep depletion devices. Even at 1 micron wavelengths for a 100 micron thick device, the QE is 20%. A detailed study of the QE of TESS CCDs is described in the accompanying work of Krishnamurthy [3].

For these deep depletion devices ($>$ 100 microns), the field generated from the gates pulling the photoelectrons to the collecting well is insufficient, leading to lateral diffusion and charge spreading for those photoelectrons generated in the deeper, field free regions. For TESS, this spreading

aggravates source confusion, where multiple stars or objects can contaminate target stars due to an increased point spread function. Because of that, full depletion is an important requirement for TESS CCDs, and it was achieved by building devices on a very high resistivity silicon (more than 5000 $\Omega \cdot$ cm) and applying voltage to the backside of the detector substrate.

The measurements described in this paper were carried out using CCID80s operated with engineering grade flight-like electronics. The CCID80 was passively cooled in a thermal vacuum chamber through thermal emission, and operated at the nominal flight temperatures of −60C. Illumination was done outside the chamber with a thermally stabilized LED operating at 660 nm wavelengths and a conjugate lens system which focused a spot from a 1 micron pinhole onto the surface of the CCD. The light intensity was varied using a pulser system which modulated the light source in a pulse train [4].

## 2 Back side depletion

We have determined the backside voltage needed to fully deplete the 100 micron region for the TESS CCDs is approximately −20V. This was verified two ways: high energy cosmic rays produce diffusion clouds along the entire path as they travel from one surface of the detector to the opposite one through the bulk of the substrate, and show a characteristic wide plume if the device has an undepleted portion [5]. A trail that is narrow along its entire length indicates that the electric field is present everywhere, and the detector is fully depleted; an example of such a trail is shown in figure 1.

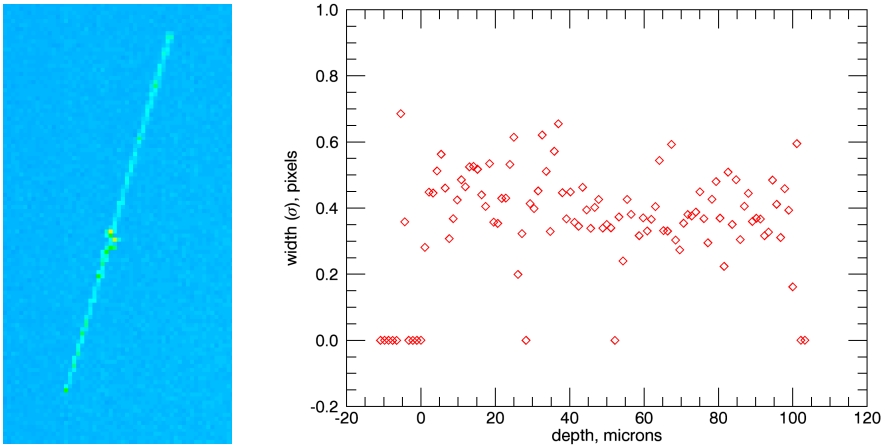


**Figure 1**. High energy cosmic rays passing through the substrate produce charge clouds at all possible depths, and can be used to estimate the depletion depth of the device. Above is an image of the trace at $V_{sub} = -25$V, and a plot of its width as a function of depth, assuming that the trace starts at the top and ends at the bottom of the detector, indicates that the CCD is fully depleted at this voltage.

A second method uses the virtual knife edge measurement, described in [6]. Here, the CCD is illuminated by an optical point source, which is moved in subpixel (< 15 micron) increments across a boundary between two pixels. By taking sums of the charge on either side of this boundary and taking the ratios between left and right, we derive a curve that displays the transition of charge



2017 JINST 12 C04025

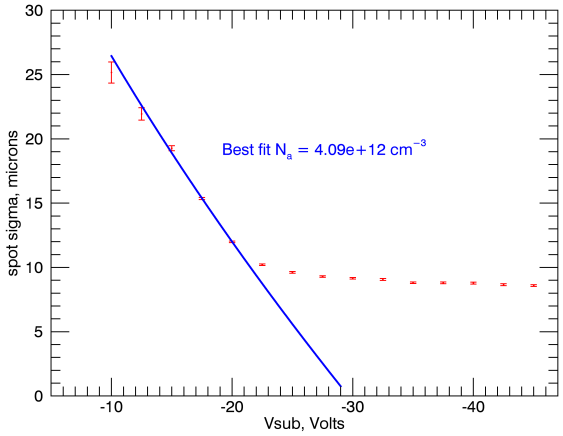


**Figure 2**. Measurement of the diffusion cloud using the Virtual Knife Edge Method

accumulation from left to right. The shape of this curve in the transition region determines the cloud radius, which is plotted as a function of substrate voltage in figure 2. There we note that the knee at which the radius stops decreasing occurs slightly above −20V, indicating full depletion of the substrate by then. The cloud radius continues to decrease with more negative substrate voltage, albeit very slowly. A blue line on the plot indicates the best fit function described by equation (13) in the S. Holland's paper [7] to the points corresponding to not fully depleted substrate. One of the results of such a fitting is a value of substrate doping level, which agrees reasonably well with nominal resistivity of 5000 $\Omega \cdot$ cm, although, we believe, that it overestimates the depletion voltage to be −30V, while in reality that is closer to −20V.

For TESS devices, we typically wish to bias at −30V or below, to ensure that our devices are fully depleted, as well as take advantage of the improving point spread function by overdepleting the device and increasing electric fields driving electrons towards collecting wells.

## 3 Anomalous behavior

We made measurements of full well capacity as a function of CCD control voltages. We can illuminate a detector with a small subpixel size spot and increase the light intensity until the pixel full well capacity is reached. Higher intensities lead to blooming along a column as excess charge spills through the gate barrier potential separating pixels in a column. The maximum charge per pixel is then achieved, which we assume to be the full well condition. Keeping the vertical low (barrier phase) voltage fixed, we can scan through various vertical high (collecting phase) voltages and determine the maximum charge in a pixel that starts to bloom. As expected, the measured full well is a linear function of vertical high voltage, as the potential well becomes deeper. This measurement was repeated at different substrate bias levels $V_{sub}$. Again as expected, full well capacity remained independent of $V_{sub}$ for levels that are not too far from full depletion point ($V_{sub}$ more positive than $\approx -30$V), as can be seen on figure 3.

However, we discovered that once $V_{sub}$ is made more negative than −30V, the full well starts to increase to nearly 250,000e-, for some settings more than double the initial capacity. We verified that this effect is not caused by gain changes in the CCD output circuit by measuring X-ray response

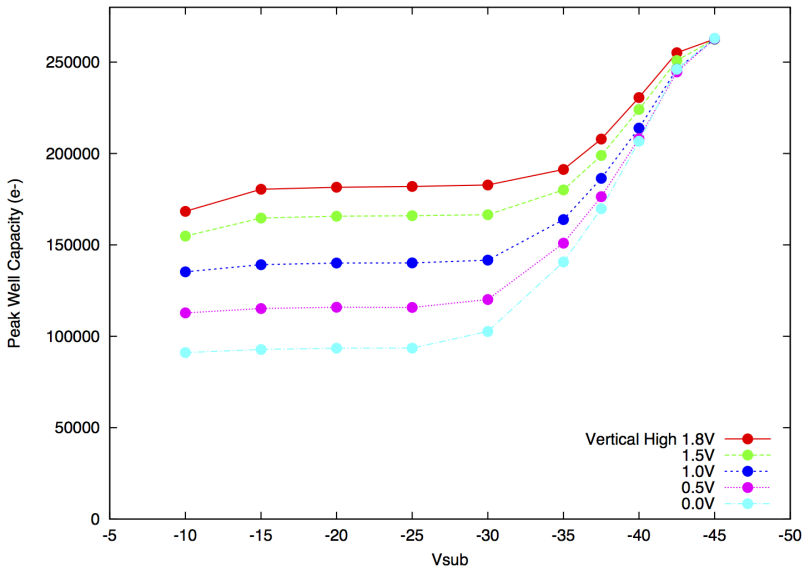


**Figure 3**. Full well voltage scans at different substrate voltages. In this series of measurements the vertical low voltage was kept at constant level of -8.0V, while the vertical high voltage was increased at half volt intervals.

at 5.9 keV. $V_{sub}$ voltage scans from −20V to −45V show a gain change of approximately 2% over that range, a tiny fraction of the corresponding change of the detector full well.

We also look at conservation of the generated photoelectric charge during the blooming process. Summing through a $100 \times 100$ pixel block centered at the spot location, we see a highly linear correspondence between the number of light pulses versus measured total charge, even for strong blooming conditions. Knowing the conversion gain, we transform the number of pulses into the total charge generated, and subtract that from the measured charge to leave the residuals indicating lost charge. We attribute this loss to surface recombination. In figure 4, we see that at $V_{sub} = -30V$ the residuals are close to zero up to many times the full well, indicating that during the blooming signal charge stays away from surface and is conserved. However, when $V_{sub}$ is set at −45V we note the loss of charge conservation, almost certainly due to surface losses.

Finally, we monitored the current flowing into the substrate during our $V_{sub}$ scans. We find that there is no current draw for $V_{sub} > -25V$, but this dramatically increases once that threshold is crossed (see figure 5).

## 4 Reach through effect

The observed behavior can be explained by a reach-through effect of the bias substrate voltage. Normally, once the substrate is fully depleted, the backside p+ layer is insulated from the frontside p+ channel stops by a potential barrier that prevents holes from flowing across the substrate. This is



2017 JINST 12 C04025

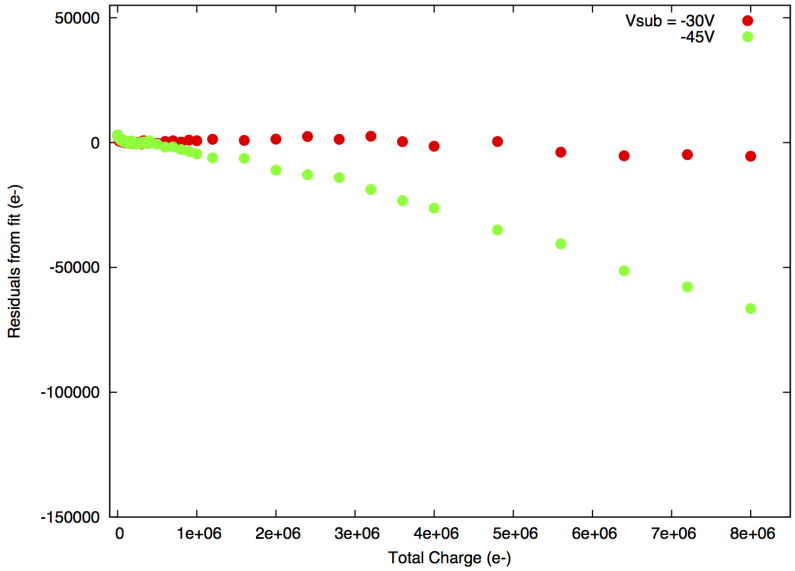


**Figure 4**. Charge conservation plots for $V_{sub} = -30V$ and $-45V$ showing the residuals from a linear fit of signal versus intensity, with downward deviations indicating surface charge loss.

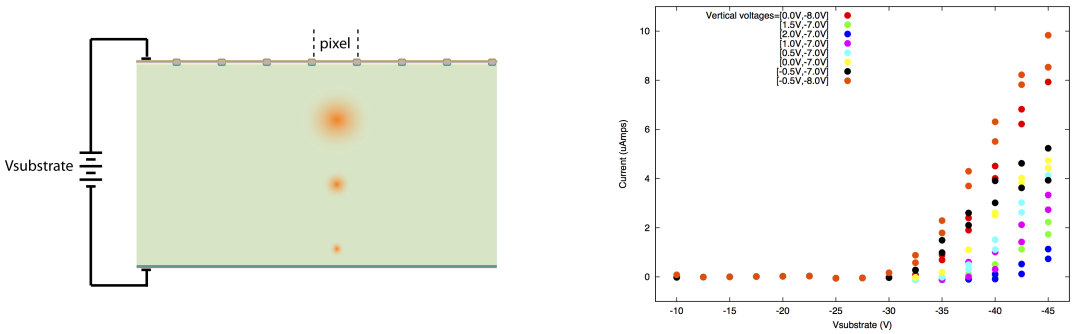


**Figure 5**. Left panel shows the bias schematic. Photons arrive from the bottom, creating charge clouds which expand as they are collected at the gates. On the right is the result of the measurement of the current draw on the substrate bias as a function of the substrate voltage, which is applied between substrate contacts on the front and back sides of the device (isolated by depleted layer).

illustrated by the top plot on figure 7, which shows schematically the potential as a function of depth at the channel stop region of a pixel. As the backside bias becomes more negative, this barrier is lowered, and eventually disappears (reach-through). Holes from channel stops may now flow to the backside contact. This progression of potential distributions is illustrated on the succeeding panels of figure 7. It should be noted that the distributions shown in both figure 7 and 8 are not simulation results, they are exaggerated cartoons serving to clarify the concept.



2017 JINST 12 C04025

The channel stops in the middle of the array in TESS CCDs are not connected to the channel stop region in the periphery (which is grounded), and hence are floating. This was because the addition of upper serial registers for charge injection in the device prevented such a connection to the grounded area. As a result, after reach-through, channel stops are pulled by the backside bias to a more negative potential, which in turn changes the inversion condition at the surface of the buried channel region.

The channel stops are the source of the holes that flow into the surface area above the buried channel, once the gate potential is negative enough to cause the inversion at the surface. When the channel stops are shifted to more negative levels, the holes will flow back out into the channel stops, and surface will get out of inversion. Such a shift leads to a less positive minimum in the barrier phase, effectively increasing the full well capacity. At the same time, the shift also allows the full well charge to get closer to the $SiO_2$ interface, causing surface charge loss when the device is in bloomed condition. The corresponding progression of the potential distributions in the middle of the pixel is illustrated in figure 8.

The floating channel stops in TESS CCDS is not a common feature. In most CCDs with channel stops held at a fixed potential the consequence of reach through would be only an increase in leakage current to the backside.

## 5 Simulations

We have carried out 3D simulation of potential distribution in the TESS CCD, using the model developed by C. Lage for LSST (see [8]) in an attempt to verify the feasibility of reach through phenomena. The plots of potential as a function of depth under the center of the collect gate in the charge storage area and channel stop region for the cases of $V_{sub} = -25V$ and $-45V$ are shown in the figure 9 below. Both distributions under collecting gate and channel stop converge within 10 microns as they approach $V_{sub}$ applied at the surface 100 microns away from the gates. For the $V_{sub} = -25V$, the barrier potential prevents holes from reaching the backside. Once $V_{sub}$ is lowered to $-45V$, this barrier almost disappears allowing holes to be collected at the backside, thus

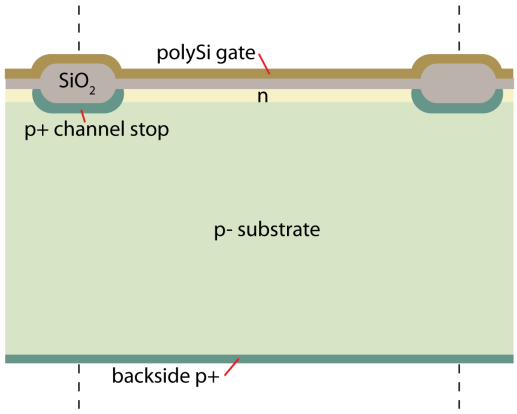


**Figure 6**. Cross section of the CCD array perpendicular to the direction of charge transfer, along the gate between two channel stops.

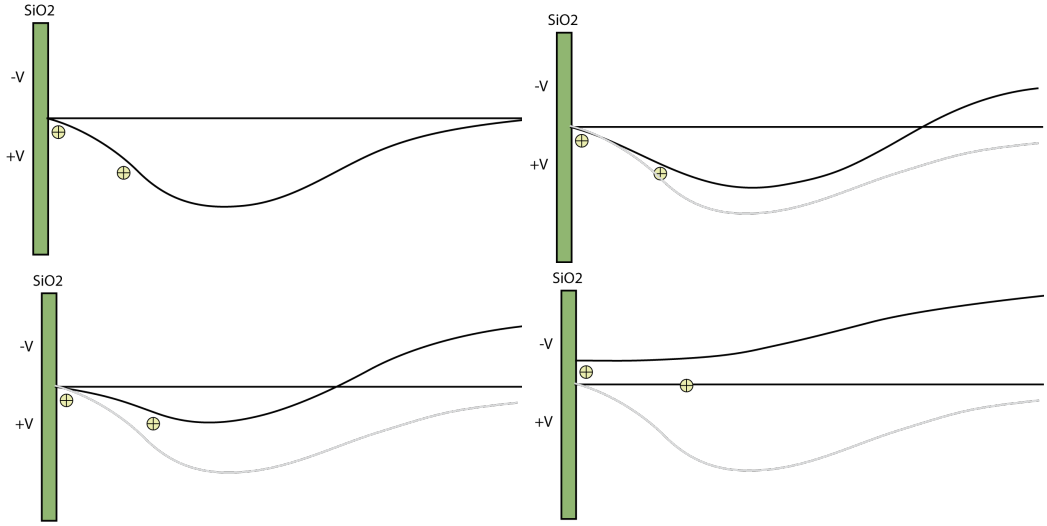


**Figure 7**. Potential profiles across the substrate passing through the channel stop center, showing the sequence as substrate bias is made more negative, starting from top left panel, moving to the most negative condition at bottom right. Note that positive potential direction is down, with depression corresponding to a barrier for holes.

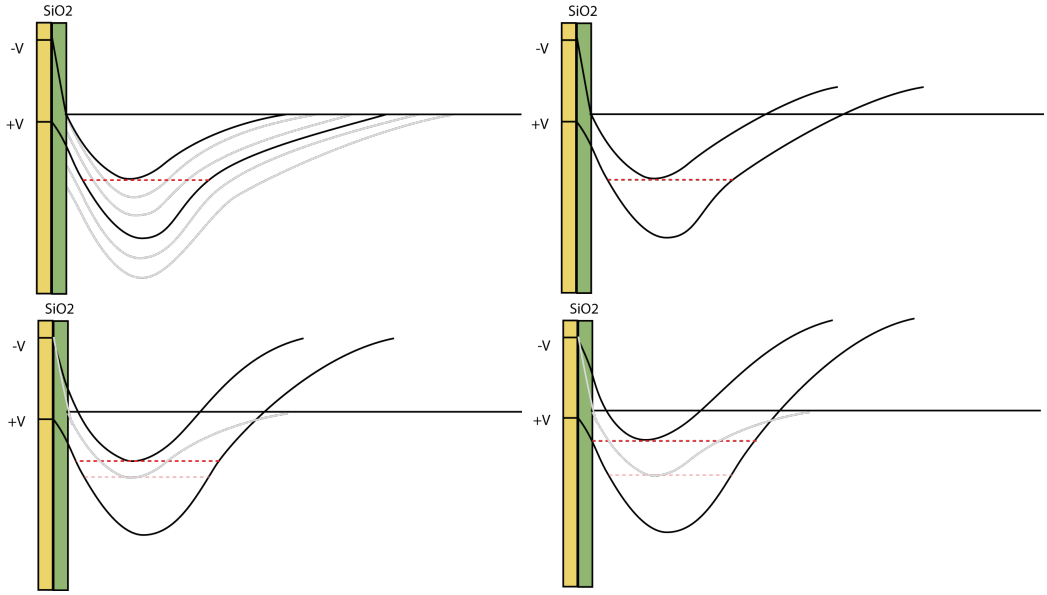


**Figure 8**. Progression of potential distributions as a function of depth under barrier and collection gates in the middle of the transfer channel as the substrate bias is decreased, starting from top left panel and progressing to the most negative bias at the bottom right panel. The four panels show the collecting and barrier potentials in solid black lines. The full well condition is shown as the red dashed line. When signal charge in the full well reaches the $SiO_2$ layer, surface recombination will lead to charge loss.

supporting the reach-through hypothesis. The distributions are sensitive to the exact geometry and doping levels of the buried channel and the channel stop, and more work is necessary to correctly include such details into the simulation. Unlike the illustration graphs on figure 8 and 7, figure 9



2017 JINST 12 C04025

is a realistic one, except for one feature: for simplicity it is assumed in the simulation that channel stop potential is grounded and cannot change, while in an actual device it is floating. Because of this, such simulation only demonstrates that reach-through effect is feasible, but does not reproduce the increase of the full well capacity observed in the experimenting with TESS devices. In the case when the channel stops are not floating, which is the case for most other CCDs, it can be expected that if a reach-through condition occurs, it would increase the current through the backside contact, and may cause voltage drop along the channel stops. But, until the current becomes really large, this may stay unnoticed, unless careful measurements of full well as a function of row number are performed.

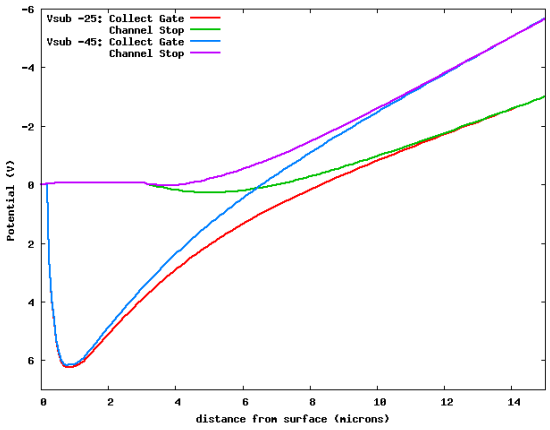


**Figure 9**. Comparison of potentials in the $V_{sub} = -25V$ and $-45V$ cases, and showing the potential profile under the collecting gate and the channel stop. These curves are the result of 3D simulation.

## 6 Summary

We have discovered somewhat unexpected behavior in the deep depletion TESS CCDs. It can be explained by a reach-through effect of the backside potential lowering the barrier for holes in the bulk of the substrate, and pulling the front side channel stops to more negative potential. To our knowledge, this behavior has not been reported previously for other CCDs. The reason could be that the reach-through condition depends on a specific combination of substrate resistivity, detector thickness, and pixel geometry. We found in simulations that the reach-through condition is especially sensitive to the channel stop parameters, such as its width and implantation depth. This may explain why other workers have been able to operate deep depletion devices at larger substrate biases than in this work.

It is our intention to operate the flight CCDs below the reach-through voltage.

## Acknowledgments

This work was supported by NASA grant NNG 14FC03C.

## References


[1] G.R. Ricker et al., *Transiting Exoplanet Survey Satellite*, *J. Astron. Telesc. Instrum. Syst.* **1** (2014) 014003 [arXiv:1406.0151].

[2] V. Suntharalingam, I. Prigozhin, D. Young et al., *Deep depletion CCD detectors for the Transiting Exoplanet Survey Satellite*, *Proc. SPIE* **9915** (2016) 28.

[3] A. Krishnamurthy, J. Villasenor, S. Kissel, R. Ricker and R. Vanderspeck, *An Optical Test Bench for the Precision Characterization of Absolute Quantum Efficiency for the TESS CCD Detectors*, submitted to JINST (2017).

[4] C. Thayer et al., *Testing and Characterization of the TESS CCDs*, *Proc. SPIE* **9915** (2016) 99042X.

[5] G. Prigozhin et al., *The Depletion Depth of High Resistivity X-ray CCDs*, *IEEE Trans. Nucl. Sci.* **45** (1998) 903.

[6] P.Z. Takacs, I. Kotov, J. Frank, P. O'Connor, V. Radeka and D.M. Lawrence, *PSF and MTF measurements for Thick CCD Sensor Characterization*, *Proc. SPIE* **7742** (2010) 774207-1.

[7] S.E. Holland, D.E. Groom, N.P. Palaio, R.J. Stover and M. Wei, *Fully Depleted, Back-Illuminated Charge-Coupled Devices Fabricated on High-Resistivity Silicon*, *IEEE Trans. Electron Devices* **50** (2003) 225.

[8] C. Lage, *Poisson_22*, https://github.com/craigslageit/Poisson_22.


2017 JINST 12 C04025